doi:10.1111/evo.12322

THE COMPLEX EVOLUTIONARY HISTORY OF SEEING RED: MOLECULAR PHYLOGENY AND THE EVOLUTION OF AN ADAPTIVE VISUAL SYSTEM IN DEEP-SEA DRAGONFISHES (STOMIIFORMES: STOMIIDAE)

Christopher P. Kenaley,[1,2] Shannon C. DeVaney,[3] and Taylor T. Fjeran[4]

[1]*Department of Organismic and Evolutionary Biology, Harvard University, Cambridge, Massachusetts 02138*

[2]*E-mail: ckenaley@fas.harvard.edu*

[3]*Life Science Department, Los Angeles Pierce College, Woodland Hills, California 91371*

[4]*College of Forestry, Oregon State University, Corvallis, Oregon 97331*

Received December 12, 2012
Accepted November 12, 2013

The vast majority of deep-sea fishes have retinas composed of only rod cells sensitive to only shortwave blue light, approximately 480–490 nm. A group of deep-sea dragonfishes, the loosejaws (family Stomiidae), possesses far-red emitting photophores and rhodopsins sensitive to long-wave emissions greater than 650 nm. In this study, the rhodopsin diversity within the Stomiidae is surveyed based on an analysis of rod opsin-coding sequences from representatives of 23 of the 28 genera. Using phylogenetic inference, fossil-calibrated estimates of divergence times, and a comparative approach scanning the stomiid phylogeny for shared genotypes and substitution histories, we explore the evolution and timing of spectral tuning in the family. Our results challenge both the monophyly of the family Stomiidae and the loosejaws. Despite paraphyly of the loosejaws, we infer for the first time that far-red visual systems have a single evolutionary origin within the family and that this shift in phenotype occurred at approximately 15.4 Ma. In addition, we found strong evidence that at approximately 11.2 Ma the most recent common ancestor of two dragonfish genera reverted to a primitive shortwave visual system during its evolution from a far-red sensitive dragonfish. According to branch-site tests for adaptive evolution, we hypothesize that positive selection may be driving spectral tuning in the Stomiidae. These results indicate that the evolutionary history of visual systems in deep-sea species is complex and a more thorough understanding of this system requires an integrative comparative approach.

KEY WORDS: **Ancestral state estimation, fossil calibration, molecular evolution, rhodopsin, spectral tuning.**

The visual pigments of vertebrates have evolved rapidly in response to selective forces in new visual environments (Yokoyama and Yokoyama 1996; Sugawara et al. 2002). The molecular mechanisms of adaptive evolution of visual pigments (i.e., spectral tuning) have been the subject of many studies in the last two decades, resulting in a better understanding of the relationships between protein sequence and pigment function (Yokoyama 2000b). Rhodopsin, the photoreceptor pigment located in the rod cells of the retina and responsible for low-light vision in vertebrates, consists of an opsin protein composed of approximately 350 amino acids that covalently bond in their secondary conformation to a chromophore, typically 11-*cis*-retinal (Menon et al. 2001). The interaction of specific amino acids of the rod-opsin protein with the pigment's chromophore constrains the absorbance peak (λ_{max}) and thus the spectral sensitivity of the pigment and the phenotype of the organism (Yokoyama and Yokoyama 1996; Menon et al.

EVOLUTION
INTERNATIONAL JOURNAL OF ORGANIC EVOLUTION

2001). Sensitive to only a very narrow wavelength of light, typically 480–490 nm (Douglas and Partridge 1997; Douglas et al. 1998a), the visual pigments of deep-sea fishes are perhaps the most specialized of all vertebrates.

Due to the optical properties of water and rapid absorption of orange-red wavelengths, sunlight is occluded, even in the clearest regions of the ocean, by about 1000 m (Warrant and Locket 2004). Because of this, and the prevalence of shortwave point-source bioluminescence produced by nearly all deep-sea taxa (Herring 1983), most mesopelagic fishes possess retinas composed only of rods cells that are most sensitive to this very narrow blue spectrum (Douglas and Partridge 1997; Douglas et al. 1998a). Therefore, as a rule, meso- and bathypelagic fishes see their world in a narrow blue spectrum, with rhodopsin phenotypes tuned to this special photic environment.

The deep-sea dragonfishes (family Stomiidae), a clade of 28 genera and more than 290 species, exemplify phenotypic adaptation to life in these dark and monochromatic waters. With an array of body and cephalic photophores and hyoid barbels that produce shortwave emissions (Herring 1983, 2007; Fig. 1A), species of the family use blue bioluminescence to communicate, lure prey, and camouflage themselves within downwelling light. The most notable exceptions to this are species belonging to the genus *Pachystomias* and the "loosejaw" dragonfish genera *Aristostomias* and *Malacosteus*. Sensitized to their own photophores that produce red emissions greater than 700 nm (Fig. 1B), these taxa have evolved extremely specialized visual pigments, some with peak absorption wavelengths greater than 650 nm (Douglas et al. 1998a). *Aristostomias* and *Pachystomias* achieve far-red sensitivity by possessing three and possibly four long-shifted rhodopsin (Partridge and Douglas 1995; Douglas et al. 1998a). In addition to rhodopsins sensitive to emissions of approximately 520 nm, these taxa use an additional porphyropsin pigment composed of the same opsin bound to 3,4-dehydroretinal (as opposed to retinal) that permits a $\lambda_{max} \approx 550$ (Bowmaker et al. 1988; Partridge et al. 1989; Partridge and Douglas 1995; Douglas et al. 1998a). In an astonishing discovery, Douglas et al. (1998b) found that *M. niger* has both a red-shifted rhodopsin-porphyropsin pair based on the same opsin protein and a photosensitizer composed of defarnesylated and demetallated derivatives of bacteriochlorophylls *c* and *d* that permits sensitivities to wavelengths greater than 630 nm.

The functional significance of these phenotypes, although untested, is apparent. Because nearly all other deep-sea taxa possess rhodopsins sensitive to only blue-shifted wavelengths, species with the capability to both produce and perceive far-red emissions are afforded a private bandwidth to communicate with conspecifics and illuminate unknowing prey. In addition, this active yet private sensory modality may extend far beyond the spatial limits of passive mechanoreception. A visual system based on long-wave emissions and sensitivity would be able to illuminate and visualize prey at a range of about 1.3 m, approximately 10 times the effective range of the lateral line system (Partridge and Douglas 1995).

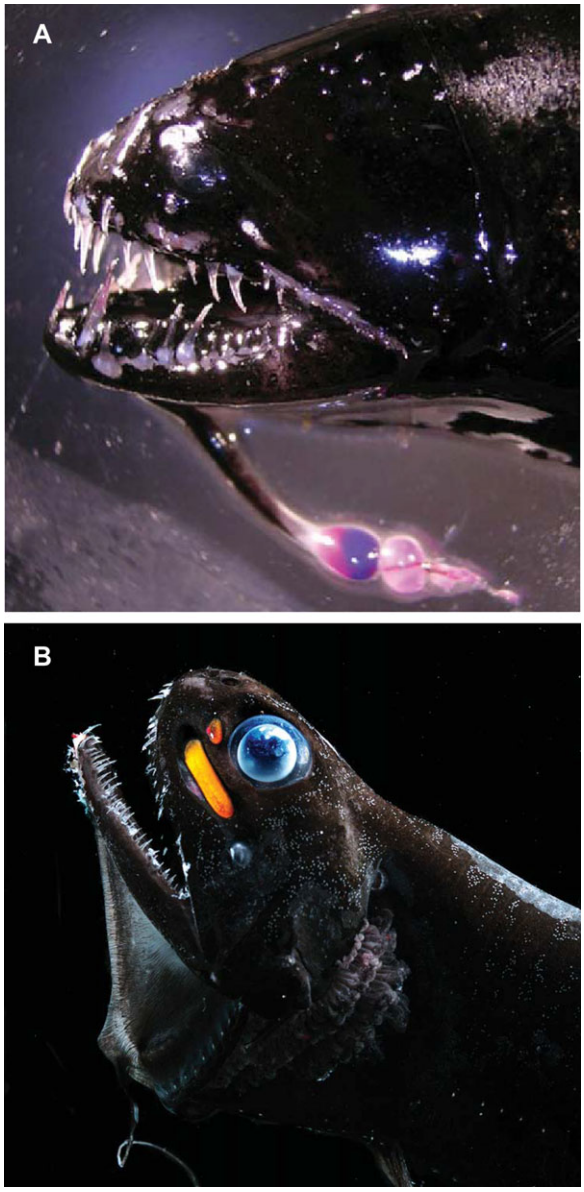

Figure 1. Representative species of the deep-sea dragonfish family Stomiidae. (A) *Echiostoma barbatum*, a species with a primitive blue-spectrum visual system (photo by senior author); (B) *Pachystomias microdon*, a species with a derived far-red visual system (photo courtesy of E. Widder).

The evolutionary history of far-red visual systems has not yet been studied in a broadly phylogenetic context. In the most comprehensive evolutionary study of spectral tuning in deep-sea fishes to date, Hunt et al. (2001) analyzed the rod opsin-coding sequences and spectral sensitivity of only five stomiid species and genera. They proposed site-specific amino acid substitutions responsible for tuning the two far-red sensitive pigments in

M. niger and two of the four in *A. tittmani*, as well as the blue-sensitive rhodopsin pigment in *Photostomias guernei* and two other stomiid species, *Idiacanthus fasciola* and *Stomias boa*. Sampling across vertebrates, Yokoyama et al. (2008) used site-directed mutagenesis of inferred ancestral rod-opsin proteins to show that 15 amino acid substitutions at 12 sites were responsible for the variation in rhodopsin absorbance, including substitutions at six functional sites responsible for far-red vision in a single species of *Aristostomias*. Neither of these two studies, however, included representatives of all four loosejaw genera or more than a few other stomiid taxa. Hunt et al. (2001) inferred amino acid substitutions within their sparsely sampled group of dragonfishes—which did not include the red-sensitive *P. microdon*, the purported sister taxon of the loosejaws (Kenaley, 2010)—by ancestral state estimation under an unspecified optimality criterion, presumably parsimony. In addition, the topology used in Hunt et al. (2001) to infer substitution histories was estimated from the opsin-coding sequences. In their study, Yokoyama et al. (2008) included only three species of dragonfishes, *Chauliodus macouni, I. antrostomus*, and the red-sensitive *A. scintillans*. Like Hunt et al. (2001) before them, Yokoyama et al. (2008) inferred ancestral states and amino acid evolution from topologies based on rod-opsin sequence data alone. It has been shown that phylogenetic trees inferred from rod-opsin sequence data alone may produce spurious reconstructions of evolutionary history (Chang and Campbell 2000). Furthermore, phylogenetic inference based on a single gene is considerably less likely to recover the true species tree than inference based on multiple loci (Knowles and Kubatko 2010 and references therein); thus, any comparative analysis based on such a topology is less likely to be accurate as well.

The focus of this study was to infer the evolutionary history of far-red sensitivity in the Stomiidae and address when and how many times this capability evolved. In addition, we sought to determine whether this intriguing phenotype evolved in response to strong selective pressure in the deep sea. To elucidate these open questions, we set out to (1) infer the phylogenetic relationships of the Stomiidae, (2) integrate our phylogenetic hypothesis with stomiiform fossil data to infer the divergences times of stomiid clades, and (3) integrate rod-opsin sequence data to infer the molecular basis and evolutionary timing of far-red sensitivity and address whether this capability is adaptive, having arisen in response to positive selection. This required a comprehensive phylogenetic approach, one that densely samples dragonfish taxa and infers evolutionary history by analyzing data from unlinked molecular loci. Our phylogenetic analysis represents the first attempt to estimate the interrelationships of the Stomiidae, the most diverse family of deep-sea fishes, based on molecular data and one of a very few studies to estimate the timing of key evolutionary events in the deep sea (e.g., Davis and Fielitz 2010). Two previous studies that analyzed a morphological dataset either failed to arrive at a fully resolved phylogenetic hypothesis (Fink 1985), or many of the relationships, particularly within the loosejaw clade, were poorly supported (Kenaley 2010).

The molecular basis of the adaptive process of spectral tuning can be uncovered in three steps (Yokoyama 2000b): (1) molecular characterization of the opsin gene, (2) identification of amino acid substitutions that are important in shifting the λ_{max} of the visual pigment, and (3) determination of the actual effects of these mutations on phenotype (i.e., λ_{max}) through in vitro analysis of the visual pigment. This last step represents a major hurdle in elucidating the molecular basis of visual adaptation in deep-sea fishes. Many deep-sea taxa are rarely captured and, due to their often distant and difficult habitat, any experimental assessment of phenotype requires extremely expensive efforts in the field. This is no doubt the reason why the λ_{max} of relatively few deep-sea fishes and stomiid species in particular have been assessed (Douglas and Partridge 1997; Douglas et al. 1998a). To address this lack of phenotypic data, we also set out on a fourth goal to predict rhodopsin phenotype of dragonfishes for which we have rod-opsin molecular data and an inferred evolutionary history of rod-opsin substitution but lack experimental λ_{max} data. We attempted to infer the λ_{max} values of these species based on phylogenetically distinct sequence motifs (PDSMs)—tuning-site sequences with the same substitution pattern according to ancestral state estimations—shared with species for which these data are available. By integrating our predictions of phenotype with previously reported λ_{max} data, the phylogenetic history of dragonfishes, and estimations of ancestral rod opsins, we set out to uncover the comprehensive history of the evolution of red visual systems in this clade of enigmatic fishes.

Methods

SEQUENCE DATA ACQUISITION

Tissue samples were taken from 57 individual fishes obtained through fieldwork or from museum material; specimens taken from the field were vouchered in museum collections (Table S1). Many of the more than 220 stomiid species are rarely captured and known from only a few specimens; however, at least one species from 25 of the 28 genera was sampled (Table S1), with *Opostomias*, *Eupogenesthes*, and *Diplostomias* unavailable. Ten species of eight basal stomiiform genera were sampled as outgroups, including members of the families Gonostomatidae, Sternoptychidae, and Phosichthyidae. Several recent molecular studies have recovered a sister relationship between the Osmeroidei and the Stomiiformes (López et al. 2004; Li et al. 2008; Near et al. 2012; Betancur-R et al. 2013), a relationship first proposed by Weitzman (1967). Thus, all trees were rooted with the osmerid *Thaleichthys pacificus*.

Tissue biopsies were taken from epaxial muscle and preserved in 95–100% ethanol directly following collection and then stored frozen at −70°C prior to DNA extraction. Total genomic DNA was extracted from tissue samples using a Qiagen DNease Tissue Extraction Kit (QIAGEN, Valencia, CA) following the manufacturer's protocol. In addition to rod opsin, three nuclear gene fragments were PCR amplified: recombination activation gene 1 (rag1); myosin, heavy chain 6, cardiac muscle, alpha (myh6); and ectodermal-neural cortex 1 (enc1). These gene fragments reflect a subset of markers analyzed now common in multilocus phylogenetic reconstruction of ray-finned fishes (e.g., Near et al. 2012, 2013; Betancur-R et al. 2013). The amplification of these additional markers proved extremely difficult and therefore was not pursued. Rod-opsin sequences were amplified with primers from Hunt et al. (2001). The other three nuclear gene fragments were amplified with the primers listed in Table S2.

PCR amplifications were carried out in 25 μl reaction volume containing 20 mM Tris-HCL, pH 8.55, 16 mM $(NH_4)_2SO_4$, 2.5–3.0 mM $MgC1_2$, 330 μM of each dNTP, 0.3 μl (1.5 U) of Biolase *Taq* polymerase (Biotin, Taunton, MA), 20 pmol of each primer, and 1.0–3.0 μl of template DNA. Rod-opsin primers amplified a ∼870 bp fragment of the intronless teleost rod opsin-coding gene that includes the seven transmembrane α-helices and associated cytoplasmic and luminal loops, regions of the protein known to interact with the chromophore and affect functionality (Menon et al. 2001), and 11 of the 12 amino acid sites identified by Yokoyama et al. (2008) as critical in tuning vertebrate rhodopsins. Nucleotides coding for site 317 were outside the amplified region. To confirm that amplified sequences were fragments orthologous to fish rod opsins, the following measures were taken: (1) to assess pairwise identity, newly generated rod-opsin sequences were compared with published sequences on GenBank. (2) Because teleost rod opsins are intronless (Fitzgibbon et al. 1995), novel sequences were screened for this feature. Lastly, (3) all novel sequences were screened for tripeptides E134, R135, and Y136 at the cytoplasmic boundary of helix 3, a pattern unique to the Stomiiformes among teleost rod opsins (Hunt et al. 2001).

For nuclear fragments other than rod opsin, any unsuccessful first-round amplification was followed by a second nested amplification. Fragments listed next to taxa in Table S1 with "-" denote unsuccessful amplification and markers not included in subsequent analyses. Successfully amplified sequences were purified using either enzymatic digestion with ExoSAP-It (USB/Affymetrix, Santa Clara, CA) or spin column purification with a QIAquick PCR Purification Kit (QIAGEN). Purified products were cycle sequenced at the University of Kansas DNA Sequencing Core Facility or University of Washington High-throughput Genomics Unit.

ALIGNMENT, SEQUENCE ANALYSIS, AND MODEL SELECTION

All novel sequences were deposited in GenBank (Table S1). Across all loci, we observed only a few putatively heterozygous sites; these and ambiguous base calls were replaced with standard IUB ambiguity codes. Each gene fragment was aligned using MUSCLE version 3.7 (Edgar 2004). Gene matrices were edited in Geneious (Drummond et al. 2009) and TextWrangler (BareBones Software). The rod-opsin matrix was further aligned by eye against mRNA sequences for *Sigmops bathyphilus* (Hunt et al. 2001) and *A. scintillans* (Yokoyama et al. 2008). Potential tuning sites were identified by first predicting amino acid residues and then annotating sites according to the functional residues identified through the directed mutagenesis study by Yokoyama et al. (2008) as critical to rhodopsin spectral sensitivity. Because identical substitutions at only a few sites have been implicated in phenotypic shifts in vertebrate rhodopsin (Yokoyama et al. 2008) and inclusion of these sites may add homoplasious artifacts to the phylogenetic signal, we followed Chang and Campbell (2000) and removed trinucleotides encoding the 11 tuning sites before phylogenetic analysis.

All four fragments were concatenated into a single matrix for analysis, yielding an aligned nucleotide dataset consisting of 3210 bp. Levels of substitution saturation were assessed for each codon position of each gene fragment using (Xia et al. 2003) substitution index in DAMBE assuming an asymmetrical topology. Substantial substitution saturation was detected at only the third-codon position of rag1 ($I_{ss} > I_{ss.cAsym}, P = 0.1231$). Thus, the third-codon position in rag1 was recoded with an RY scheme whereby purines (A and G) were recoded as "R" and pyrimidines (C and T) recoded as "Y." For this partition, the substitution model imposed a single rate category (lset nst = 1) instead of six (lset nst = 6) to allow the software to estimate only transversional changes between purine and pyrimidine nucleotides. The dataset was further partitioned by gene and codon position for all four gene fragments, totaling 12 partitions. For the remaining 11 partitions, nucleotide substitution models were chosen under the Akaike Information Criterion (AIC) as calculated in MrModelTest version 2.2 (Nylander 2004); models assigned to each partition are give in Table S3.

PHYLOGENETIC INFERENCE

Phylogenetic analyses were performed under a Bayesian optimality criterion as implemented in MrBayes version 3.2 (Ronquist and Huelsenbeck 2003). We undertook six mixed-partitioned analyses: one for each gene fragment, an analysis excluding rod-opsin data, and an analysis of a concatenated matrix of all four loci. In each analysis, model parameters for all partitions were unlinked and priors for model parameters were set to default values (topology: uniform, revmat: dirichlet (1.0, 1.0, 1.0, 1.0, 1.0, 1.0), statefreq: dirichlet (5.0, 5.0, 5.0, 5.0), pinvar: uniform (0.0, 1.0),

brlengths: exp (10.0), shape: uniform (0, 1)). Each analysis implemented two runs with three heated and one cold Markov chains. Each Markov chain Monte Carlo (MCMC) run commenced for 20 million generations and was sampled every 1000 generations, for a total of 20,000 sample trees. All parameters had effective sample sizes (ESSs) greater than 200, thus each MCMC run had at least several hundred independent samples. To insure that the sample captured the target distribution of trees, convergence of the chains was assessed by graphical inspection of the state likelihoods, potential scale reduction factors, and the average deviation of the split frequencies. A sample of the first 5000 trees was discarded as burn-in. A 50% majority-rule consensus tree was inferred from the remaining post burn-in samples. Clade support in the form of posterior probabilities (pps) was calculated from all post burn-in trees. Topologies for each analysis other than the inference of the full dataset are presented in Figures S1–S5.

ESTIMATION OF DIVERGENCE TIMES

Divergence times for stomiiform lineages were estimated by implementing an uncorrelated lognormal model (UCLN) of molecular evolutionary rate heterogeneity in the program BEAST (version 1.7.4; Drummond et al. 2006; Drummond and Rambaut 2007). The data matrix was partitioned by locus and codon position according to the same models implemented in the Bayesian analyses with all partition parameters unlinked. To accommodate RY coding for the third-codon position of rag1, we removed the operator on kappa in the XML input file and set the initial value to 0.5. A Yule-birth speciation prior was implemented for the branching rates. The concatenated Bayesian topology was used as a starting tree. To accommodate node-age priors in the BEAST analysis, the Bayesian topology was time calibrated by estimating node ages with Sanderson's (2002) penalized-likelihood method implemented in the "chronopl" program of R's APE package (Paradis et al. 2004; R Core Team 2012). The absolute age estimates from the five calibration priors outlined below constrained the same five nodes as minimum ages. For this starting-tree calibration with chronopl, the smoothing parameter (lambda) was arbitrarily set to 0.1 with all other settings aside from minimum age left at their default values.

We ran four independent MCMC analyses of 50×10^6 generations each, sampling every 5000 generations. MCMC convergence was assessed by visualizations of the state likelihoods TRACER version 1.5 (Rambaut and Drummond, 2007). As with our MrBayes inference, all parameter ESS values were greater than 200, indicating adequate mixing of the MCMC analyses. The analysis produced a total of 40,000 chronograms, of which 10,000 were discarded as burn-in with the remaining 30,000 used to generate a maximum clade-credibility tree with TreeAnnotator version 1.7.5 (beast.bio.ed.ac.uk/TreeAnnotator). The mean and 95% highest posterior density (HPD) estimates of divergence times were visualized over the maximum clade credibility tree in R.

A secondary calibration based on Near et al. (2012) and four fossil stomiiform taxa were used to assign age calibration priors in the UCLN analysis. For fossil-calibrated nodes (calibrations 2–4), the fossil taxa used to calibrate these nodes, characters supporting placement of each fossil taxon in the phylogeny, stratigraphic information of the formations bearing the fossils, absolute age estimates, and prior age settings in the BEAST analysis are described below. Soft upper bounds for each fossil calibration were calculated using Marshall's (2008) FA_c at a confidence level of 0.95.

Calibration 1. Crown clade Stomiiformes + Osmeroidei. We implemented a secondary calibration based on Near et al.'s (2012) estimate of divergence time for the Stomiiform-osmeroid node. A prior with normal distribution was assigned to this node with a mean = 141 Ma and standard deviation (SD) = 16.4 Ma. This distribution reflects the 95% HPD estimate for divergence time of this node in Near et al. (2012) with a 95% confidence interval of 114–168 Ma.

Calibration 2. Crown lineage Stomiiformes. The fossil stomiiform †*Paravinciguerria praecursor* from the black shales of the Argille Varicolori, northeastern Sicily, represents the first occurrence of the order (Carnevale and Rindone 2011). The Argille Varicolori formation represents deposits from the lower portion of Oceanic Anoxic Event 2 in the late Cenomanian (Scopelliti et al. 2008). This permits an absolute age estimate of 93.5 ± 0.8 Ma, the late Cenomanian–Turonian boundary. In their examination of *Paravinciguerria*, the most comprehensive to date, Carnevale and Rindone (2011) found no characters to support placement of *Paravinciguerria* in any of the recognized stomiiform clades and, thus, treated this taxon as a stem stomiiform despite its lack of any unambiguous apomorphies that unite the Stomiiformes according to Fink and Weitzman (1982) and Harold and Weitzman (1996). Instead, Carnavale and Rindone (2011) relied on other characters to assign *Paravinciguerria* to the Stomiiformes, namely: premaxilla short with a reduced ascending process; maxilla elongate with a rounded and gradually curving profile; maxillary teeth small and closely spaced, of subequal length; and supramaxilla elongated posteriorly and coming to a single pointed terminus. A lognormal prior was assigned to this node in the UCLN analysis with a mean = 3.33 and SD = 0.8 to set the minimum offset to 93.5 Ma and the soft upper bound to 197.7 Ma.

Calibration 3. Stem lineage Sternoptychinae, dating the most recent common ancestor (MRCA) of *Sternoptyx pseudobscura*, *Argyropelecus aculeatus*, and *A. gigas*. An unassigned species of the sternoptychid subfamily Sternoptychinae (sensu Harold and Weitman 1996) from the Lutetian–Bartonian boundary (absolute age estimate of 40.4 ± 0.2 Ma; Luterbacher et al. 2004) represents the first occurrence of the subfamily in the fossil record

(G. Carnevale, unpubl. ms., 2013). The following character states support the placement of this taxon within the subfamily: body discoid, frontal crest prominent, parietal crest present, opercle elongate and subrectangular, subopercle roughly triangular, hyomandibula greatly elongate, posttemporal elongate and strongly ossified, and neural spine of the second preural centrum broad and flat. A lognormal prior was assigned to this node in the UCLN analysis with a mean = 2.48 and SD = 0.8 to set the minimum offset to 40.4 Ma and the soft upper bound to 84.6 Ma.

Calibration 4. Stem lineage *Chauliodus*, dating the MRCA of *C. sloani* and *C. danae*. The Miocene †*C. eximius* from the Yorba Member of the Puente Formation in southern California represents the first occurrence of the genus in the fossil record (Crane 1966). Huddleston and Takeuchi (2013) assigned an upper Mohnian age (7.6–8.6 Ma) to the Yorba Member based on diatom flora. The following character states support the placement of *C. eximius* within the genus: enormous anterior dentary and premaxillary fangs present, dorsal-fin origin at anterior third of body, and second dorsal-fin ray modified as an extremely elongate filament. A lognormal prior was assigned to this node in the UCLN analysis with a mean = 0.82 and SD = 0.8 to set the minimum offset to 7.6 Ma and the soft upper bound to 20.6 Ma.

Calibration 5. Crown clade *Borostomias* + *Rhadinesthes*. An unassigned species of the genus *Borostomias* from the Middle Miocene (Serravallian) of Torricella Peligna, Abruzzo, Italy, represents the first record of this clade (Carnevale 2007). Based upon published biostratigraphic data, Carnevale (2007) assigned a minimum age of 12.6 Ma to the deposits at Torricella Peligna. The following character states support the placement of Carnevale's (2007) †*Borostomias* sp. within the genus: Type 1 tooth attachment and maxilla unserrated. A lognormal prior was assigned to this node in the UCLN analysis with a mean = 1.323 and SD = 0.8 to set the minimum offset to 12.6 Ma and the soft upper bound to 26.6 Ma.

ROD-OPSIN ANCESTRAL STATE RECONSTRUCTION

Ancestral states for each deduced amino acid residue at 11 of the 12 critical tuning sites identified by Yokoyama et al. (2008) were reconstructed under a marginal-likelihood criterion implemented in the phangorn package for R (Schliep 2011). An LG model of amino acid substitution (Le and Gascuel 2008) was identified as best fitting with ProtTest 3 (Darriba et al. 2011) under AIC. This model was optimized for the Bayesian tree with "pml" in phangorn and implemented in marginal-likelihood reconstructions. Species for which rod-opsin amplification was unsuccessful were pruned from the phylogeny. Custom R scripts were used to visualize the probabilities of the inferred ancestral amino acid reconstructions (Appendix S1).

SPECTRAL TUNING AND INFERENCE OF RHODOPSIN PHENOTYPE

The effect of amino acid substitution at the 11 amplified tuning sites throughout the evolution of the dragonfish lineage on spectral sensitivity was assessed by incorporating phenotypic data (λ_{max}) from the studies listed in Table 1. For species without reported λ_{max} values, phenotype was predicted based on tuning-site genotypes (i.e., sequence motifs) and evolutionary history shared with species for which data are available. Incorporating a "vertical" strategy in which ancestral substitutions at functional sites within a protein are used to infer the relationship between genotype and phenotype is now recognized as important and more informative than inference based on comparing contemporary genotypes alone (Harms and Thornton 2010). A vertical approach that uses the evolutionary history of functional sites to engineer ancestral proteins has been useful in elucidating the particular amino acid substitutions important in the tuning of vertebrate photoreceptors (Yokoyama 2000a; Yokoyama et al. 2007, 2008). To infer rhodopsin sensitivities for species without phenotypic data, we extended this vertical approach by scanning through the ancestral nodes for every species in the trimmed tree to identify the most recent substitutions at each of the identified tuning sites. For species without phenotype data, we estimated phenotype by scanning the tree for species with phenotype data and identical substitution histories. The λ_{max} values of species sharing these PDSMs were assembled to establish a distribution of phenotype values for each PDSM. As an upper and lower limit of inferred phenotype, the minimum and maximum λ_{max} values of each PDSM were then assigned to species without phenotypes according to its shared PDSM. This algorithm was implemented with "pheno.tip," a custom R script given in Appendix S2. To assess how well the most common PDSMs ($n \geq 3$) predict phenotype, we applied a generalized linear model using R's "glm" function, assuming a normal error distribution ("family = gaussian").

TESTS FOR ADAPTIVE EVOLUTION

To determine whether far-red sensitivity arose as a result of positive selection, we inferred rates of nonsynonymous (d_N) and synonymous (d_S) substitutions in rod opsin-coding sequences throughout the Bayesian topology via maximum-likelihood estimations implemented in PAML's CODEML program (Yang 2007). The ratio of d_N/d_S (ω) is >1 under positive selection and approaches 1 under neutral selection. Under this framework, we implemented a series of likelihood ratio tests (LRTs) in which we compared the log-likelihood of alternative to null branch and branch-site models in CODEML. First, we compared the alternative branch model that permits ω of the foreground lineage (i.e., a clade of red-sensitive taxa) to vary relative to the background (i.e., the remainder of the blue-sensitive stomiiform clades) against the null model that does not vary across the

Table 1. Peak spectral absorbance (λ_{max}) data of rhodopsin photoreceptor pigments for species of the family Stomiidae and stomiiform outgroup taxa and the corresponding phylogenetically distinct sequence motif of their rod-opsin sequence.

Species	λ_{max}	Source	PDSM
Vinciguerria nimbaria	477	Fernandez (1979)	1
Sigmops elongatum	482	Bowmaker et al. (1988)	2
Sigmops bathyphilus	481	Partridge et al. (1989)	2
Triplophos hemingi	*480–487*	*Predicted*	*2*
Sternoptyx pseudobscura	479	Partridge et al. (1989)	3
Argyropelecus aculeatus	477	Partridge et al. (1988)	4
Argyropelecus gigas	477	Partridge et al. (1988)	4
Polymetme thaeocoryla	*480–487*	*Predicted*	*2*
Yarrella blackfordi	Unknown		5
Ichthyococcus ovatus	489	Partridge et al. (1992)	6
Chauliodus danae	484	Partridge et al. (1989)	7
Chauliodus sloani	485	Partridge et al. (1988)	6
Stomias atriventer	489	Fernandez (1979)	8
Heterophotus ophistoma	*480–487*	*Predicted*	*2*
Rhadinesthes decimus	480	Partridge et al. (1989)	2
Astronesthes gemmifer	*480–487*	*Predicted*	*2*
Chirostomias pliopterus	487	Douglas and Partridge (1997)	2
Trigonolampa miriceps	*480–487*	*Predicted*	*2*
Flagellostomias boureei	*480–487*	*Predicted*	*2*
Leptostomias gladiator	*480–487*	*Predicted*	*2*
Tactostoma macropus	*480–487*	*Predicted*	*2*
Echiostoma barbatum	483	Partridge et al. (1989)	2
Idiacanthus fasciola	485	Partridge et al. (1989)	6
Photonectes braueri	483	Douglas and Partridge (1997)	2
Photonectes margarita	*480–487*	*Predicted*	*2*
Melanostomias bartonbeani	*480–487*	*Predicted*	*2*
Grammatostomias flagellibarba	480–487	*Predicted*	*2*
Bathophilus pawneei	480–487	*Predicted*	*2*
Bathophilus vaillanti	*480–487*	*Predicted*	*2*
Pachystomias microdon	520, 563,[1] 595	Douglas et al. (1998a)	9
Malacosteus niger	522, 548[1]	Bowmaker et al. (1988)	9
Aristostomias scintillans	526, 551[1]	O'Day and Fernandez (1974)	9
Aristostomias tittmanni	531, 548,[1] 588	Partridge and Douglas (1995)	9
Photostomias guernei	483	Hunt et al. (2001)	10
Eustomias polyaster	Unknown		11
Eustomias filifer	Unknown		12

[1] A_2-based porphyropsin.

Italic values for λ_{max} indicate inferred phenotypes.

topology. If an LRT indicated that the alternative branch model was best fitting, we undertook a second LRT that compared an alternative branch-site model of selection in which sites within the foreground branches are under positive selection ($\omega > 1$) against the null model that the sites in the foreground lineage are under neutral selection ($\omega = 1$). The LRT statistic was calculated as follows: $2\Delta L = 2(L_1 - L_0)$, where L_0 is the log-likelihood of the null model with p_0 parameters and L_1 is the likelihood of the alternative model with p_1 parameters. Values for $2\Delta L$ were compared to a χ^2 distribution with $p_1 - p_2$ degrees of freedom.

Results

PHYLOGENETIC RELATIONSHIPS WITHIN THE FAMILY STOMIIDAE

Our analyses in MrBayes and BEAST resulted in the same topology for the Stomiidae and selected outgroups (Fig. 2). We inferred a paraphyletic Stomiidae with *Chauliodus* sister to *Ichthyococcus*, a nonstomiid of the paraphyletic family Phosichthyidae. Support for the *Chauliodus–Ichthyococcus* relationship is rather strong (pp > 0.94). A clade of the remaining Stomiidae and major relationships within the family received strong support in our

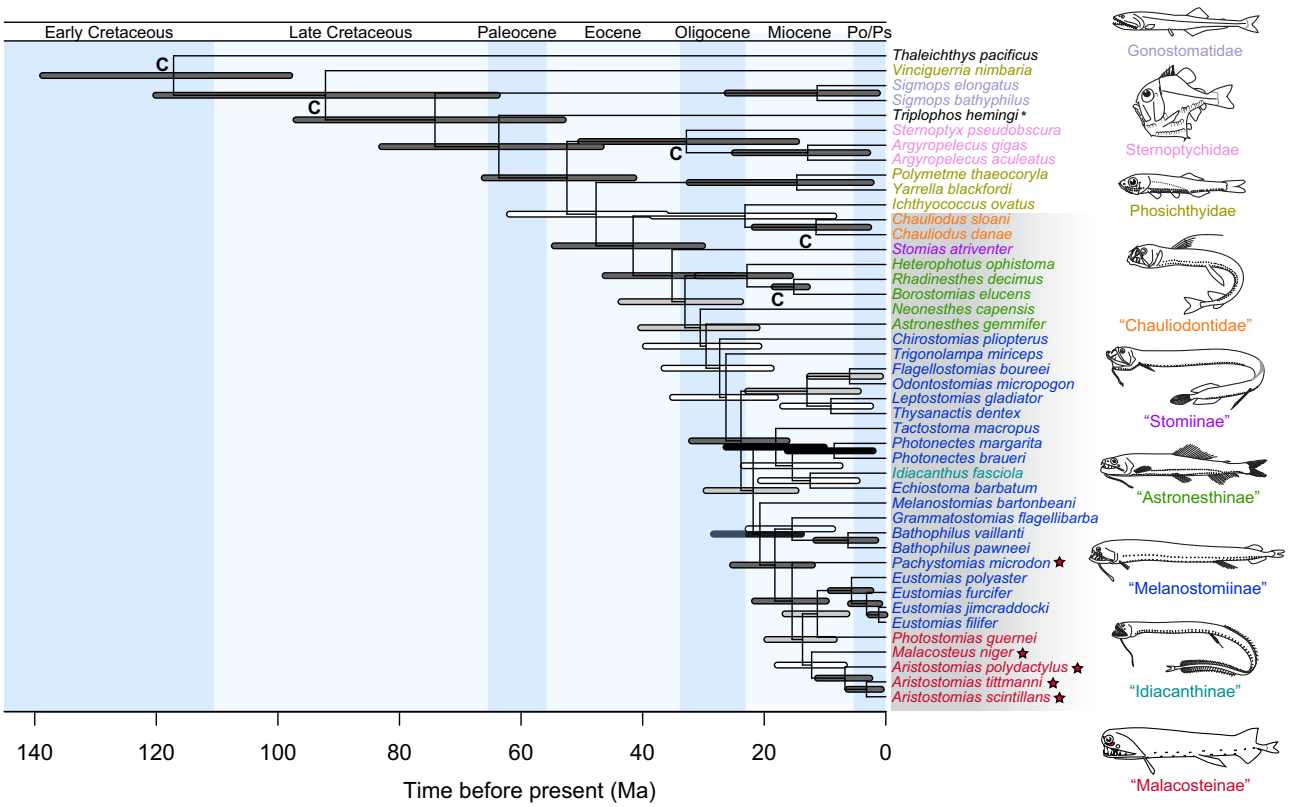

Figure 2. **Time-calibrated phylogeny based on four nuclear loci and four fossil age constraints. The topology represents a 50% majority-rule consensus of the posterior distribution in the MrBayes analysis and maximum clade-credibility tree from the analysis in BEAST. Bars over nodes represent 95% highest posterior density intervals of age estimates. Dark gray bars indicate Bayesian posterior probabilities (pps) of 1.0, light gray 0.95 ≤ pp < 1, and white pp < 0.95. Nodes calibrated with fossil-age estimates are labeled with "C." Terminal taxa within the gray box represent the Stomiidae; taxa marked with a red star indicate far-red sensitive species. Color of the terminal taxa correspond to subfamilial designations listed to the right; an asterisk indicates Stomiiformes *incertae sedis*.**

analyses. The type genus *Stomias* was recovered as sister to the remaining dragonfish genera. A clade containing the "astronesthine" genera *Heterophotus, Borostomias*, and *Rhadinesthes*, with the latter two taxa recovered as sister to one another, was resolved as sister to a clade of the remaining stomiids. In stepwise fashion, the remaining astronesthines *Neosnesthes* and *Astronesthes*, and the monotypic "melanostomiines" *Chirostomias* and *Trigonolampa* are each in turn sister to clades containing the balance of stomiid taxa. Four elongate melanostomiine genera, *Flagellostomias*, *Odontostomias*, *Leptostomias*, and *Thysanactis*, comprised a clade sister to the remainder of the dragonfishes. We inferred that the balance of the Stomiidae is composed of two subclades: one consisting of the monotypic genus *Tactostoma* sister to a clade of *Photonectes*, which is in turn sister to *Echiostoma* and *Idiacanthus*. The other is composed of *Melanostomias* sister to a clade of *Grammatostomias* + *Bathophilus* which is, in turn, sister to a paraphyletic loosejaw clade that includes the three malacosteine genera plus *Eustomias* and *Pachystomias*. This well-supported *Eustomias–Pachystomias*-loosejaw clade (EPL hereafter) comprises the monotypic *Pachystomias* as sister to a group composed of the malacosteines *Malacosteus* and *Aristostomias* sister to the malacosteine *Photostomias* and melanostomiine *Eustomias*.

DIVERGENCE TIME ANALYSIS

Based on our relaxed-clock analysis in BEAST, we estimated that the MRCA of the stomiiform-osmeroid clade arose at the end of the Early Cretaceous at 117.3 Ma (95% HPD = 98.5–139.4 Ma; Fig. 2). Diversification of the crown Stomiiformes began at 91 Ma (63.1–119.6 Ma) in the middle of the Late Cretaceous (Fig. 2). The MRCA of the Stomiidae senso stricto (minus *Chauliodus*) arose in the late Eocene at 34.9 Ma (24.9–45.7 Ma). We estimated that divergence for the EPL clade, the lineage containing all the far-red sensitive taxa, began at 15.4 Ma (9.9–21.4 Ma) in the Early to Middle Miocene (Fig. 2). Our estimated divergence time for the MRCA of the clade containing *Eustomias–Photostomias* was 11.2 Ma in the Middle to Late Miocene (Fig. 2).

ROD-OPSIN AMPLIFICATION, EVOLUTION, AND SPECTRAL TUNING

The fragments amplified were confirmed as orthologous vertebrate rod opsins. Several sequences amplified in this study, including *A. tittmanni*, *A. scinctillans*, *M. niger*, *S. elongatum*, *S. bathyphilus*, and *Vinciguerria nimbaria* are identical to those amplified for these same species by other researchers studying rhodopsins in deep-sea fishes (Hunt et al. 2001; Yokoyama et al. 2008). All of the novel sequences are intronless, a feature of teleost rod opsin (Fitzgibbon et al. 1995). In addition, all novel sequences contained a conserved tripeptide at the cytoplasmic boundary of helix 3 in the form of E134, R135, and Y136, a pattern unique to the Stomiiformes among fish rod opsins (Hunt et al. 2001).

Ten of the 11 potential tuning sites at the focus of this study were polymorphic; no changes at site 122 occurred throughout the phylogeny of the stomiids and the selected outgroups (Table 2). Marginal-likelihood reconstructions for each of the 10 polymorphic sites are presented in Figure S6. Ancestral state reconstructions of the most likely states for these 11 critical sites are summarized as tuning-site substitution histories on the inferred topology in Figure 3. Diversity at functional sites in the Stomiidae and outgroup basal stomiiforms was remarkably low, totaling only 20 changes across the 11 potential tuning sites (Table 2). Nine of the 20 substitutions occurred in a single lineage, the EPL clade. Half of the substitutions can be accounted for at two sites, 289 and 292, the former constituting the most labile site with six amino acid substitutions across the phylogeny and the latter with four. Residues 122, 183, 253, and 261 changed twice across the topology, whereas 83, 96, 194, 195 underwent a single substitution each.

Both substitutions at residues and 253 and 261 occurred in the EPL clade: M253L and F262Y in the MRCA of these taxa and reversals L253M in the MRCA of *E. filifer* and *E. polyester*, and Y261F in the MRCA of *Photostomias* and *Eustomias* (Fig. 3C). Three of the four substitutions at site 292 occurred in the EL clade as well; S292I at the root, I292T in *Photostomias*, and a reversal of T292S in *Eustomias*. A unique substitution, T289G, occurred at the root of the EL clade. Five other substitutions at site 289 were all T289A, occurring in several basal stomiiform taxa, *C. sloani*, and *I. fasciola* (Fig. 3B, C). M183F occurred both at the base of the EL lineage and in *V. nimbaria*. A parallel substitution E122Q occurred in *V. nimbaria* and in the MRCA of the sternoptychids (Fig. 3C). Single substitutions N83D, Y96W, R194Q, and A195D occurred in *S. atriventer*, *S. pseudobscura*, *V. nimbaria*, and *C. danae*, respectively.

Phenotypic data for rhodopsin sensitivity (λ_{max}) were available for 20 of the 36 taxa for which rhodopsin sequences were amplified or available from GenBank (Table 1). For 13 of the 16 taxa without data, we uncovered genotypes and inferred tuning-site histories shared with taxa for which λ_{max} data were available, permitting prediction of phenotype in these species (Fig. 3, Table 1). This PDSM (motif 2, $n = 6$) was a significant predictor of phenotype among species with known blue-sensitive phenotypes of 480–487 nm ($P < 0.001$; Fig. 4). PDSM 6 ($n = 3$), which included taxa with λ_{max} 483–489 nm (Table 1), did not predict phenotype significantly better than PDSM 2 ($P = 0.194$; Fig. 4). Thus, through our PDSM analysis, we were able to infer that all of these 13 species posses rhodopsin photoreceptors sensitive to blue wavelengths between 480–489 nm (Table 1).

The two species of *Eustomias* included in this study have either incomplete sequence data in the case of *E. polyaster* or a unique sequence and tuning-site substitution history in the case of *E. filifer* and thus, phenotype could not be inferred for these species. Sequence data for *Yarrella blackfordi*, a basal stomiiform, was also incomplete, preventing a prediction of phenotype. The tunings sites that did amplify for *Y. blackfordi*, however, are identical to the ancestral rod opsin.

Our combined analyses of phylogenetic and phenotypic inference and reconstructions of rod opsin-coding sequences predicted that far-red visual systems evolved once within the Stomiidae in the MRCA of the EL clade. The tuning-site genotypes and substitution histories of *Malacosteus*, *Aristostomias*, and *Pachystomias*, the only taxa with far-shifted (>520 nm) rhodopsin phenotypes, are unique to species of these genera. Elsewhere in our phylogeny, all other stomiid and basal stomiifrom taxa possess shortwave, blue-sensitive rhodopsins, or rod-opsin genotypes and substitution histories associated with λ_{max} below 490 nm. This includes *Photostomias* and most likely *Eustomias*, sister taxa nested within a clade of red-sensitive dragonfishes. *Photostomias guernei* possesses a rhodopsin tuned to 483 nm (Hunt et al. 2001). Our analysis predicted that this reversal is achieved by only two substitutions, I292T and Y261F. These tuning events occurred at the root of the EL clade and, thus, indicate a single reversal to a near-shifted visual system within the EL lineage. Because the species of *Eustomias* included in this analysis possess unique tuning-site genotypes and substitution histories, we could not make a confident prediction of phenotype for these taxa. To our knowledge, no mutagenesis studies have investigated the effects of the two substitution at the base of the *Eustomias* clade, L253M and T292S. These substitutions represent reversals to the primitive genotypes at these sites. Although reversals to primitive genotypes may result in reversals to primitive phenotype (Sugawara 2005), it is not always the case (Yokoyama et al. 2008). However, that species of *Eustomias* possess primitive genotypes at some sites and have evolved from an ancestor sensitive to blue wavelengths indicates that these taxa also possess blue visual systems.

Table 2. Inferred amino acid residues at potential tuning sites in stomiiform rod opsins.

	Site										
Species	83	96	102	122	183	194	195	253	261	289	292
MRCA of all taxa	N	Y	Y	E	M	R	A	M	F	T	S
Vinciguerria nimbaria	.	.	.	Q	F	Q	.	.	.	.	.
Gonostoma elongatum	.	.	.	.	.	.	.	.	.	.	.
Sigmops bathyphilus	.	.	.	.	.	.	.	.	.	.	.
Triplophos hemingi	.	.	.	.	.	.	.	.	.	.	.
Polymetme thaeocoryla	.	.	.	.	.	.	.	.	.	.	.
Yarrella blackfordi	.	.	.	.	.	.	.	.	.	?	?
Sternoptyx pseudobscura	.	W	.	Q	.	.	.	.	.	A	A
Argyropelecus aculeatus	.	.	.	Q	.	.	.	.	.	A	.
Argyropelecus gigas	.	.	.	Q	.	.	.	.	.	A	.
Ichthyococcus ovatus	.	.	.	.	.	.	.	.	.	A	.
Chauliodus danae	.	.	.	.	.	.	D	.	.	.	.
Chauliodus sloani	.	.	.	.	.	.	.	.	.	A	.
Stomias atriventer	D	.	.	.	.	.	.	.	.	.	.
Astronesthes gemmifer	.	.	.	.	.	.	.	.	.	.	.
Heterophotus ophistoma	.	.	.	.	.	.	.	.	.	.	.
Rhadinesthes decimus	.	.	.	.	.	.	.	.	.	.	.
Chirostomias pliopterus	.	.	.	.	.	.	.	.	.	.	.
Trigonolampa miriceps	.	.	.	.	.	.	.	.	.	.	.
Flagellostomias boureei	.	.	.	.	.	.	.	.	.	.	.
Leptostomias gladiator	.	.	.	.	.	.	.	.	.	.	.
Tactostoma macropus	.	.	.	.	.	.	.	.	.	.	.
Echiostoma barbatum	.	.	.	.	.	.	.	.	.	.	.
Idiacanthus fasciola	.	.	.	.	.	.	.	.	.	A	.
Photonectes braueri	.	.	.	.	.	.	.	.	.	.	.
Photonectes margarita	.	.	.	.	.	.	.	.	.	.	.
Melanostomias bartonbeani	.	.	.	.	.	.	.	.	.	.	.
Grammatostomias flagellibarba	.	.	.	.	.	.	.	.	.	.	.
Bathophilus pawneei	.	.	.	.	.	.	.	.	.	.	.
Bathophilus vaillanti	.	.	.	.	.	.	.	.	.	.	.
Pachystomias microdon	.	.	.	.	F	.	.	L	Y	G	I
Malacosteus niger	.	.	.	.	F	.	.	L	Y	G	I
Aristostomias scintillans	.	.	.	.	F	.	.	L	Y	G	I
Aristostomias tittmanni	.	.	.	.	F	.	.	L	Y	G	I
Photostomias guernei	.	.	.	.	F	.	.	L	F	G	T
Eustomias polyaster	.	.	.	.	F	.	.	.	F	?	?
Eustomias filifer	.	.	.	.	F	.	.	.	F	G	.

Residues indicated by "." are identical to the most common recent ancestor (MRCA) of all taxa. Missing data are indicated by "?".

TESTS FOR ADAPTIVE EVOLUTION

Our phylogenetic analysis and reconstructions of spectral-tuning events reveal that far-red sensitivity evolved once in the Stomiidae in the MRCA of the EPL clade. Thus, we undertook a single two-part assessment of positive selection. Likelihood models that permit a different selection regime (i.e., a discrete value for ω) and the presence of sites under positive selection within the EPL clade fit the data significantly better than the corresponding null models (Table 3). In our first LRT for selection, a branch model that allowed ω of rod-opsin amino acid sites in the foreground EPL clade to vary from the background was chosen over the null model in which ω was constant across our topology ($P < 0.001$; Table 3). In our second LRT for selection, a branch-site model in which sites within the foreground EPL clade were under positive selection ($\omega > 1$) was chosen over the null model in which selection in the foreground lineage was neutral ($\omega = 1$; $P < 0.001$; Table 3). Sites under positive selection (i.e., those with probabilities greater than 0.95 that $\omega > 1$) included sites

183, 292. Our tests reveal that three additional tuning sites, 253, 261, 289, were under selection, however, probabilities of $\omega > 1$ were not significant ($P > 0.05$). Estimates of ∞ for ω indicate that some of these sites underwent only nonsynonymous substitutions in the EPL clade (data not shown; Yang and Reis 2011).

Discussion

SUMMARY

Our results render the Stomiidae and the loosejaw dragonfishes—the Malacosteinae—paraphyletic. Integrating available rhodopsin phenotype data and inference of phenotype based on PDSMs with our topology, we hypothesize that, aside from species of *Aristostomias*, *Malacosteus*, and *Pachystomias*, all stomiids sampled have rhodopsins sensitive to short wave, blue wavelengths with λ_{max} below 490 nm. Despite the nonmonophyly of the Stomiidae and red-sensitive taxa, ancestral state reconstructions over our inferred topology reveal that the amino acid substitutions permitting far-red sensitivity have evolved once in the Stomiidae in the MRCA of a clade comprising *Eustomias*, *Pachystomias*, and the loosejaw genera *Aristostomias*, *Malacosteus*, and *Photostomias*. From our divergence time analysis, we estimated that the crown group stomiids (minus *Chauliodus*) originated 34.9 Ma (Fig. 2). A period of some 20 million years spans the origin of the crown stomiids to the origin of the clade containing all the red-sensitive taxa, the EPL clade, at 15.4 Ma in the middle Miocene (Fig. 2). This expanse of time in the evolutionary history of the Stomiidae is characterized by no spectral tuning in rhodopsin despite relatively high taxonomic diversification (Fig. 3). It was within the EPL lineage that we inferred the highest number of critical amino acid substitutions that alter rhodopsin phenotype, including substitutions that have led to a reversal back to the plesiomorphic blue-sensitive phenotype (Fig. 3). Through codon-based estimations of ω, we hypothesize that, within the EPL clade, at least two amino acids critical to rhodopsin phenotype have been subject to positive selection (Table 3).

INTERRELATIONSHIPS OF STOMIID GENERA

The phylogenetic hypothesis inferred by our analysis differs in several important aspects from other phylogenetic treatments of the Stomiidae. The most notable difference is that both Fink (1985) and Kenaley (2010) recovered a monophyletic Stomiidae, while this study inferred a sister relationship between the stomiid *Chauliodus* and the phosichthyid *Ichthyococcus* (Fig. 2). We also inferred novel relationships at the base of the stomiid tree with sequential sister relationships to remaining stomiid taxa between *Stomias*, a clade of the "astronesthine" genera *Heterophotus*, *Borostomias*, and *Rhadinesthes*, *Neonesthes*, *Astronesthes*, *Chirostomias*, and *Trigonolampa*, in that order (Fig. 2). Fink (1985) and Kenaley (2010) recovered *Neosesthes* as the sister taxon to all other stomiids, followed by a polytomy composed of *Astronesthes*, *Borostomias*, divergence of a clade comprising *Heterophotus* and *Rhadinesthes*, divergence of a clade composed of *Chauliodus* and *Stomias*, followed by divergence of a *Chirostomias–Trigonolampa* clade that is sister to the balance of the stomiids. Within the *Grammatostomias–Bathophilus* + EPL clade, the outstanding differences between this hypothesis and previous studies concern the placement of *Eustomias* and the interrelationships of the "malacosteine" loosejaw taxa. Both the morphological studies of Fink (1985) and Kenaley (2010) proposed a monophyletic loosejaw + *Pachystomias* clade sister to a clade containing *Eustomias*, *Grammatostomias*, and *Bathophilus*, where our analysis supports a *Eustomias* + *Photostomias* clade nested within the a lineage comprising *Pachystomias* and the remaining loosejaw genera *Malacosteus* and *Aristostomias* (Fig. 2).

Before Fink's (1985) phylogenetic analysis of the group, the taxa now contained within the Stomiidae were distributed among five families (see Fink, 1985:3–8). Since that study, many authors still recognize these nonmonophyletic groups as stomiid subfamilies (i.e., Stomiinae, Chauliodontinae, Melanostomiinae, Idiacanthinae, and Malacosteinae; Nelson 2006; Eschmeyer 2013). Our study corroborates the para- or polyphyletic hypotheses for these subfamilial groups; therefore, we must discourage the application of these taxonomic concepts in future studies.

SPECTRAL TUNING AND EVOLUTION OF LONG-WAVE SENSITIVITY

This study is the first to show that the evolution of a red visual system from a primitive blue system is a single evolutionary event in the dragonfishes (Fig. 3). By integrating an estimation of ancestral rhodopsin evolution with previously reported phenotypic data and our predictions of phenotype based on shared PDSMs, we inferred that molecular innovations at tuning sites and correlated phenotypic shifts to far-red sensitivity occurred only once within the dragonfishes at the base of the EPL clade. Based on our UCLN analysis in BEAST, we estimated that this shift to far-red sensitivity took place 15.4 Ma in the middle Miocene (Fig. 2). As predicted by analysis of shared PDSMs and indicated by λ_{max} from other studies, we inferred that all taxa outside the EPL clade possess rhodopsins sensitive to blue spectra (Fig. 3). We also inferred that, within the EPL clade, the MRCA *Photostomias* and *Eustomias* re-evolved a blue visual system approximately 11.2 Ma in the Middle to Late Miocene, reverting back to the primitive sensitivities possessed by other, non-EPL dragonfishes and stomiiforms (Figs. 2, 3). These spectral tuning events represent two extraordinary shifts in phenotype within a relatively short span of 4 millions years. This suggests that the evolutionary history of visual systems of fishes inhabiting the deep sea may be more complex and labile than would be suggested by the relatively stabile photic environment of the deep sea.

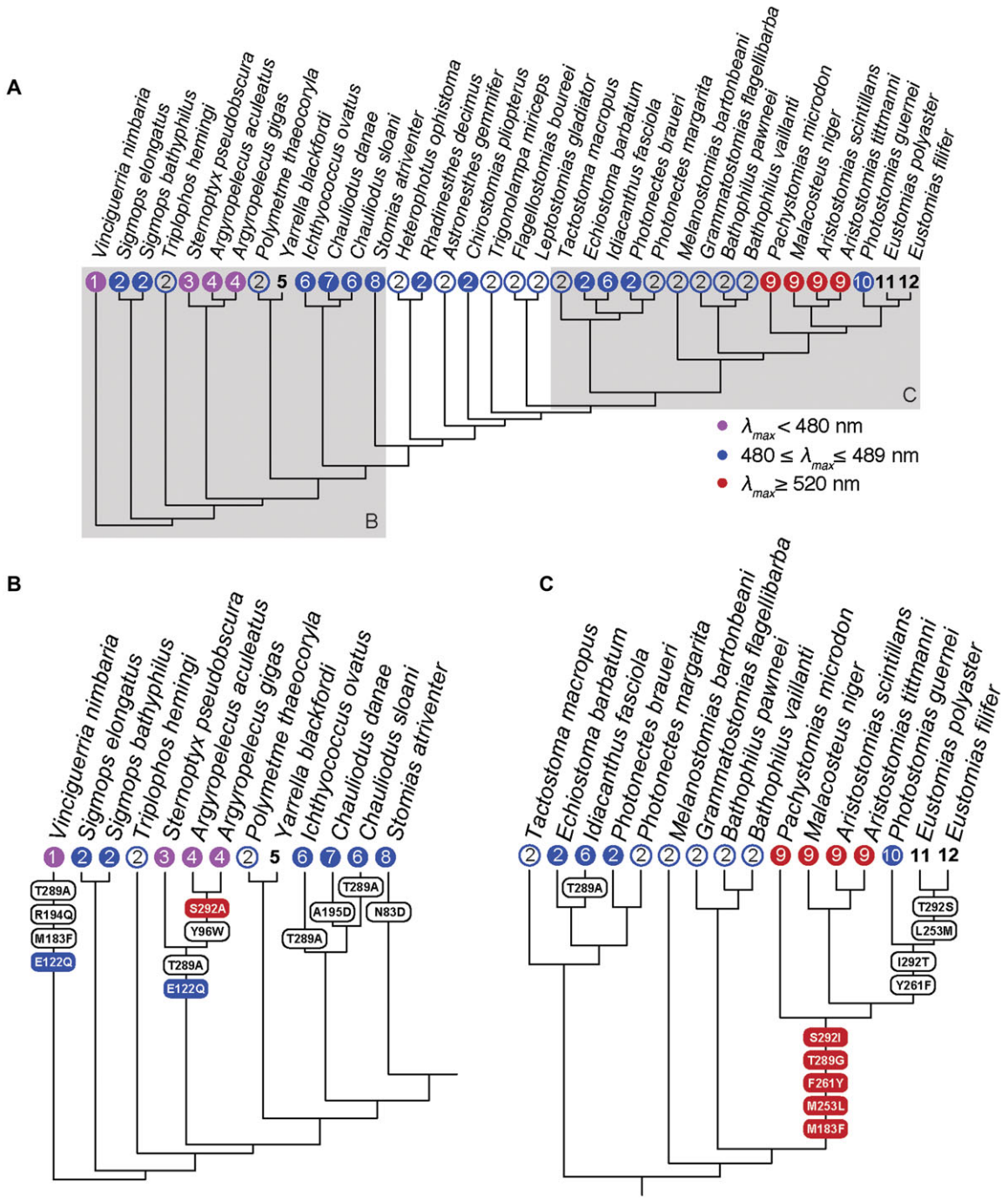

Figure 3. Reconstruction of amino acid substitutions at 11 rod-opsin tuning sites and the effect on rhodopsin sensitivity in the deep-sea dragonfish family Stomiidae and selected outgroup taxa. (A) Pruned topology represented in Figure 2 to include only those taxa with rod-opsin sequence data. (B, C) Shaded areas of the phylogeny in (A) represented in detail. Boxes on the branch lengths correspond to specific amino acid substitutions inferred from maximum-likelihood estimations of ancestral states (see Fig. S6). Red- and blue-colored boxes represent substitutions known to produce red and blue shifts in peak absorbance (λ_{max}) of vertebrate opsins, respectively. White boxes correspond to substitutions for which the effect on λ_{max} has not been evaluated. Circles at the tips of the phylogeny represent values for λ_{max}. Solid circles correspond to experimental values obtained from the literature: purple λ_{max} < 480 nm, blue 480 nm ≤ λ_{max} < 489 nm, red λ_{max} > 520 nm. Open blue circles correspond to values predicted by phylogenetically distinct sequence motifs (PDSMs) of the 11 tuning sites (480 nm ≤ λ_{max} ≤ 487 nm). Numbers correspond to shared PDSMs. Tips labeled with only a number represent species for which no experimental data exist and predictions could not be made.

Only two other deep-sea fishes, both of the family Myctophidae, have been found capable of perceiving far-red wavelengths: *Myctophum nitidulum* and *Bolinichthys longipes* (Hasegawa et al. 2008; Turner et al. 2009). Because myctophids do not produce red emissions from their photophores, Hasegawa et al. (2008) and Turner et al. (2009) suggested that red sensitivity in these species may be an adaptation to perceive the far-red emissions of red-capable stomiid dragonfishes, important predators of myctophids in meso- and bathypelagic ecosystems (Sutton and Hopkins 1996b). *Myctophum nitidulum* achieves red sensitivity via an unpaired porphyropsin pigment and *B. longipes* via a chlorophyll-based photosensitizer (Hasegawa et al. 2008; Turner et al. 2009). Because of the dissimilar mechanism by which these two myctophids perceive long-wave spectra, it is clear that the evolution of far-red sensitivity in the two taxa are separate evolutionary events. In addition, these two events did not involve tuning of the rod-opsin gene. Thus, the red shift in the MRCA of the EPL clade represents the only known example in fishes of far-red sensitivity achieved through tuning and molecular evolution in the rod-opsin gene.

The singular shift to far-red sensitivity in the Stomiidae can be explained by five amino acid substitutions that occurred at the base of the EPL lineage: M183F, M253L, F261Y, T289G, and S292I (Fig. 3B). Not surprisingly, these substitutions constitute a PDSM that is a strong predictor of far-red phenotypes ($\lambda_{max} \approx$ 520 nm; $P < 0.001$; Fig. 4). Hunt et al. (2001) first suggested that two of these (F261Y and S292I) were responsible for sensitivity to spectra beyond approximately 520 nm in *Aristostomias* and *Malacosteus*. Using directed mutagenesis techniques, Yokoyama et al. (2008) demonstrated that all five of the transitions at the base of the EPL clade produce a red shift in λ_{max} and that these very transitions are responsible for a $\lambda_{max} \approx 520$ nm in *A. scintillans*. The results of these studies and ours that estimated PDSMs among the long-wave sensitive taxa indicate that a red visual system with a $\lambda_{max} \approx 520$ evolved in the MRCA of the EPL clade.

Our branch-site tests indicate that positive selection may, in part, be driving spectral tuning in the EPL clade. We detected positive selection at two of the critical tuning sites, 183 and 292 ($P < 0.05$; Table 3). We also detected selection at another three tuning sites, 253, 261, and 289, in the EPL clade; however, probabilities that these sites were under selection were not significant ($P > 0.05$; data not shown). Identifying what may be responsible for adaptive evolution at tuning sites requires some speculation due to the fact that very little is known about the ecology of these species. However, there are several aspects of the morphology and behavior of far-red species that differ substantially from the majority of stomiid species. First, the hyoid barbel is absent or this structure is simple and lacks the complexity that is the hallmark morphology of many other dragonfishes (e.g., see Morrow and Gibbs 1964). Second, unlike most species within the

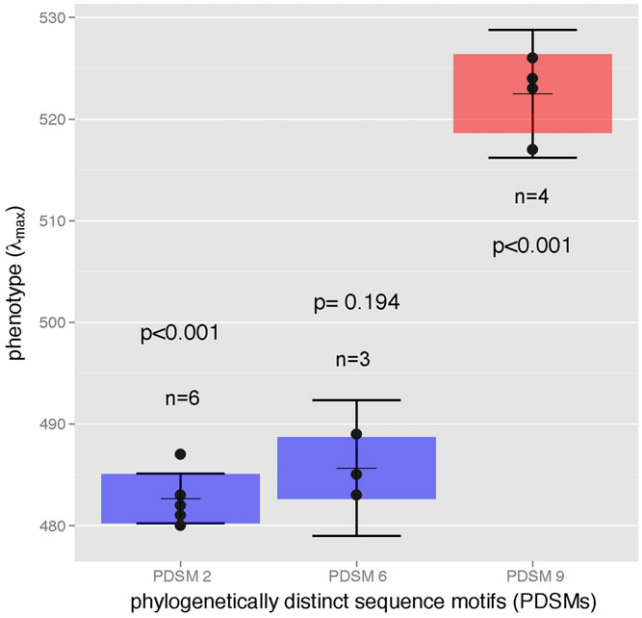

Figure 4. Box plot of the three most common phylogenetically distinct sequence motifs versus retinal sensitivity. Shaded boxes correspond to the standard deviation with blue and red representing near- and far-sensitive phenotypes, respectively. Small dashed lines and whiskers correspond to the λ_{max} estimates and the 95% confidence interval, respectively.

family, the red-sensitive stomiids either do not undergo regular diel vertical migrations or migrate very sporadically from extreme depths (Sutton and Hopkins 1996a; Kenaley 2008). Taken together, these idiosyncrasies may reflect a shift from the pervasive foraging strategy within the family based on chasing a raft of prey to the epipelagic at night and, while there, luring individual prey with blue-emitting hyoid barbels and detecting prey with blue-sensitive photoreceptors. We expand upon the hypothesis proposed by Partridge and Douglas (1995) and suggest that far-red stomiids evolved a foraging strategy based on remaining at depth and, rather than luring with a complex barbel, scanning a short field with far-red wavelengths undetectable by nearly all other prey species. The innovation of a foraging strategy that relies on far-red emissions required concomitant innovations in retinal sensitivity. This, we suggest, is the force that drove spectral tuning and adaptive evolution in the visual systems of the far-red stomiids. Indeed, there is very strong covariation between photoreceptor sensitivity and maximum wavelength of bioluminescence across the majority of deep-sea taxa for which both spectral tuning and emission data exist (Douglas et al. 1998a and references therein).

With regards to *Aristostomias*, *Malacosteus*, and *Pachystomias*—red-sensitive taxa with photophore emissions exceeding 700 nm—the evolution of a rhodopsin with $\lambda_{max} \approx$ 520 is not adequate to explain their full phenotypic range

Table 3. Likelihood ratio tests of positive selection along branches and sites within rod opsin-coding sequences of stomiid dragonfishes according to CODEML (Yang, 2007).

Model class	Model	ln*L*	Parameters	Parameter estimates for ω					Positive sites	2Δln*L*	*P*
	Single ω	−7879.2	72	ω=0.1310					NA		
Branch	Discrete ω (background ω_0 and foreground ω_1)	−7903.3	73	ω_0=0.1228 ω_1=1.4190					NA	14.7	<0.001
	Null model A: neutral selection in foreground lineage	−7445.3	74	Class	0	1	2a	2b	NA		
				Proportion	0.78	0.16	0.05	0.01			
				Background ω	0.05	1.00	0.05	1.00			
				Foreground ω	0.05	1.00	1.00	1.00			
Branch site	Alternative model A: positive selection in foreground lineage	−7440.0	75	Class	0	1	2a	2b	183, 292	10.56	<0.001
				Proportion	0.81	0.16	0.02	0.01			
				Background ω	0.05	1.00	0.05	1.00			
				Foreground ω	0.05	1.00	∞	∞			

Test 1 evaluated a branch model of selection in which the alternative hypothesis that ω (d_N/d_S) in the foreground lineage (i.e., the EPL clade) was discrete from the background lineages (the remainder of the stomiiform clades) against the null that ω does not vary across all stomiid lineages ("model = 0" and "nsites = 0" vs. "model = 2" and "nsites = 0," respectively). Test 2 evaluated a branch-site model of selection in which the alternative hypothesis that sites within the foreground branches are under positive selection (ω > 1) was compared to the null hypothesis that the sites in the foreground lineage are under neutral selection (ω = 1; "model = 2, NSsites = 2, fix_omega = 1," and "omega = 1" vs. "model = 2, NSsites = 2, fix_omega = 0," and "omega = 1.5," respectively). Positive sites listed indicate those with *P* < 0.05.

(Table 1). Authors of other studies have shown that to achieve sensitivities beyond approximately 520 nm, these taxa use an additional porphyropsin pigment composed of the same opsin bound to 3,4-dehydroretinal (as opposed to retinal) that permits a $\lambda_{max} \approx 550$ (Bowmaker et al. 1988; Partridge et al. 1989; Partridge and Douglas 1995; Douglas et al. 1998a). Because this rhodopsin-porphyropsin pair is based on the same opsin, the results of our study also indicate that the $\lambda_{max} \approx 550$ also evolved at the base of the EL clade. However, the maximum emissions of the red photophores of these taxa well exceed the λ_{max} values of this pigment pair. Partridge and Douglas (1995) and Douglas et al. (1998a) found that *A. tittmanni* and *P. microdon* possess a third pigment composed of another opsin with retinal as the chromophore that had a $\lambda_{max} \approx 588$–595 (Table 1). Although this pigment represents the most long-wave shifted rhodopsin ever characterized, it is a rather inexact match with the most long-wave emissions of these taxa and, thus, Douglas et al. (1995) and Douglas et al. (1998) proposed the existence of a complimentary porphyropsin that would have a $\lambda_{max} \approx 670$ nm.

The presence of two rhodopsin-porphyropsin pairs indicates a gene duplication event, possibly a tandem duplication, at the base of the EL clade or within each of these lineages. Opsin gene duplications have played an important role in the phenotypic diversification of the visual systems in many vertebrates and especially fishes (Rennison et al. 2011). Therefore, the diversity of the phenotypes of these fishes may be attributed to as many as three evolutionary mechanisms: gene duplication, alternative chromophore utilization, and spectral tuning. In addition, a characterization of the gene encoding the opsin in the extremely far-shifted rhodopsin-porphyropsin pair may reveal as yet undiscovered molecular mechanisms that permitted such dramatic shifts in phenotype.

Perhaps the most extraordinary aspect of the visual systems of dragonfishes is the mechanism by which *M. niger* achieves long-wave sensitivity beyond 520 nm. In addition to photopigments, the outer segments of the rod cells of this species contains an additional photostable pigment that absorbs light at approximately 670 nm and isomerizes one of the less red shifted photopigments (Bowmaker et al. 1988). Remarkably, this photosensitizer is

composed of chlorophyll-based compounds that have a dietary origin (Douglas et al. 1998b). In a sense, this photosensitizer stands in place of the additional, extremely long-wave shifted rhodopsin-porphyropsin pair possessed of *Aristostomias* and *Pachystomias*. Our reconstructions of tuning-site history reveal that this photosensitizer isomerizes a rhodopsin photopigment ancestral to the EPL clade and, thus, this represents another pathway in the evolution of a far-red visual systems within this relatively closely related group of fishes: alternative chromophore utilization, spectral tuning, and isomerization via a photosensitizer.

Because the MRCA of the EPL clade possessed a red-sensitive rhodopsin, the position of blue-sensitive *Photostomias* and *Eustomias* as sister taxa nested within the EPL clade reveals an amazing reversal in the phenotype and visual system in the ancestor of these taxa. Our analysis indicates that the *Photostomias–Eustomias* lineage reverted back to primitive sensitivities through transitions I292T and Y261F, and that perhaps further tuning in *Eustomias* was achieved through additional substitutions L253M and T292S (Fig. 3C). Because we lack phenotypic data for any of the species of *Eustomias* included in this study and these taxa have unique tuning-site PDSM within our sample of stomiiforms, we cannot confidently predict the phenotype of *E. polyaster* and *E. filifer.* Despite this, the balance of available data suggests that these species also possess rhodopsins sensitive to near-shifted spectra. Of these, only Y261F has been implicated in phenotypic shifts of opsin sensitive—approximately 10 nm to the blue (Yokoyama 1995). I292T, L253M, and T292S have not been reported in previous studies of tuning in vertebrate opsins and its effect on rhodopsin λ_{max} has not been examined in mutagenesis studies. These latter three substitutions may represent novel molecular pathway in the acquisition of blue-shifted phenotypes.

As it is for the far-red sensitive taxa, it is hard to speculate as to the selective pressures that would have led to a convergent acquisition of blue sensitivities in the EPL clade. Here again, the strong covariation between a species' photoreceptor sensitivity and its maximum bioluminescent wavelength must be implicated. The ability to produce far-shifted luminescence was lost in the *Eustomias–Photostomias* clade. Both taxa possess sexually dimorphic cephalic photophores (Herring 2007), including a blue-emitting accessory photophore in *Photostomias*, this is a purported homolog of a far-red emitting in *Pachystomias* (Kenaley 2010). The genus *Eustomias* contains approximately 120 species diagnosed almost exclusively on the basis of hyoid barbel morphology. These structures, thought to be important in luring prey, are the most ornate within the family, with bulbous photophores and fiber-optic-like filaments, and may represent the most morphologically diverse luminescent systems among bioluminescent taxa. The emission maxima of the barbel of species of *Eustomias* and the cephalic photophores of species of both genera have yet to be characterized. However, many qualitative observations of freshly caught specimens of the genus by the current authors and others (e.g., Gibbs et al. 1983) indicate that the barbels and cephalic photophores of species of *Eustomias* produce shortwave luminescence. Therefore, it appears that blue luminescent systems are important in luring prey and communicating with conspecifics in species of *Photostomias* and *Eustomias*, and that these behaviorally important morphologies may represent the correlative selective force behind a reversal to a primitive blue visual system.

Our results also show that the tuning history across our inferred phylogeny resulted in only minor shifts in phenotype (Fig. 3). Outside of the EPL clade there were only five substitutions within the Stomiidae senso lato. The remaining eight substitutions occurred in only two lineages, the sternoptychid clade and *V. nimbaria*. Substitution T289A was most widespread, comprising nearly one-quarter (five) of the 21 total substitutions on the topology and over a third of the 13 substitutions outside the EL clade (Fig. 3). The effect of T289A on tuning the λ_{max} of vertebrate opsins has not been established; however, Piechnick et al. (2012) found that this mutation resulted in slower release of retinal from binding sites during photoactivation of rhodopsin and a modest reduction in the uptake of retinal during rhodopsin regeneration. Despite this and the recurrence of the substitution, our results indicate that it has little or no effect on the sensitivity of stomiiform rhodopsin. Three species possess this one substitution in their tuning-site histories (Fig. 3B, C; Table 1), however the range of λ_{max} values for these three taxa is 483–489 nm, which is within the range of the phenotype of the inferred ancestral rhodopsin. Similarly, A195D occurred in *C. danae*, the only tuning site divergent from the ancestral rhodopsin in this species (Fig. 3B). However, the λ_{max} of *C. danae* is 485 nm, a value also within the range of the ancestral rhodopsin. Therefore, A195D likely caused very little to no shift in phenotype.

Lastly, we note that our phylogenetic topology that was the basis for inferring the evolutionary history of spectral tuning in the Stomiidae differs from the topologies of Hunt et al. (2001) and Yokoyama et al. (2008). In both these previous studies, phylogenies of the study group were inferred from analysis of a single molecular marker, the rhodopsin sequence data itself. Each included many fewer stomiid taxa than the present study, however both recovered a similar phylogenetic pattern with respect to one another in that *Idiacanthus* and either *Stomias* or *Chauliodus* shared an MRCA to the exclusion of *Aristostomias*. These relationships are incongruous with our phylogenetic hypothesis of these genera and those of the two previous phylogenetic reconstructions of the family (Fink 1985; Kenaley 2010). In addition, Hunt et al. (2001) recovered sister relationships between *Ichthyococcus* and a clade of sternoptychids and *Sigmops* and *Vinciguerria*, hypotheses that differ markedly from our own and other studies based on comprehensive morphological datasets (Harold and

Weitzman 1996; Harold 1998). The one-marker strategy of Hunt et al. (2001) and Yokoyama et al. (2008) exposes phylogenetic analysis to all the bias associated with that one locus and, thus, the analysis is less likely to infer the tree true as compared to analyses of unlinked loci (Knowles and Kubatko 2010 and references therein). Phylogenetic analysis based on rhodopsin sequence data has been shown to recover spurious relationships, often with high levels of clade support (Chang and Campbell 2000). In addition to the biasing mutational properties pointed out by Chang and Campbell (2000) (e.g., base and amino acid composition biases), our study and several others including Hunt et al. (2001) and Yokoyama et al. (2008) have demonstrated the convergent evolution of genotype. These biases may be responsible for some of incongruent relationships in Hunt et al. (2001) and Yokoyama et al. (2008). Reconstructions of ancestral characters over a topology are only as accurate as the topology itself. Spurious nodes never existed and thus, in the case of mutagenesis studies, neither did inferred proteins at spurious nodes. For these reasons, we caution future researchers studying the evolution of protein function, and specifically vertebrate photoreceptors, to avoid relying on the protein under study as the sole source of phylogenetic data.

In conclusion, our results indicate that the evolution of far-red visual systems was a singular event within the family Stomiidae and that a clade of dragonfishes that share a MRCA with far-red sensitive taxa reacquired a primitive blue visual system. We also have uncovered the evolutionary history of the molecular genetic mechanisms responsible for much of the phenotypic variation in far-red dragonfishes and have identified potentially novel molecular mechanisms responsible for spectral tuning in deep-sea fishes. As other studies focusing on different taxa have demonstrated, relatively few changes at rhodopsin tuning sites are responsible for rather large shifts in phenotype and parallel amino acid substitutions are responsible for convergent evolution of phenotype within relatively closely related taxa. Furthermore, through relaxed-clock dating of our inferred topology, we hypothesize that for more than half the initial evolutionary history of the Stomiidae these fishes maintained plesiomorphic rhodopsin phenotypes. It was approximately 15 Ma that far-red sensitivity evolved in the EPL clade, only to revert back to blue sensitive in the MRCA of an EPL subclade 4 million years later. This complex history of stasis, reversals, parallelism, and convergence underscores the lability of vertebrate visual systems and indicates that, despite a near uniform photic environment, fishes inhabiting Earth's largest ecosystem have repeatedly explored new adaptive pathways. We also demonstrate that a phylogenetic comparative approach, like the one taken in this study, has predictive potential. By reconstructing the evolutionary history of functional sites within rhodopsin coding sequences and scanning our topology for taxa with identical PDSMs and known λ_{max} values, we made phylogenetically informed predictions of phenotype, filling in gaps of our knowledge for rare and experimentally difficult species. Likewise, such an approach may permit researchers to identify potentially novel and testable molecular pathways that are the basis of adaptive changes in phenotype. Although there is an immense value to mutagenesis studies that employ a similarly vertical approach (i.e., integrating data from ancestral genotype and phenotype to elucidate relationships between the two; e.g., Yokoyama et al. 2008), phylogenetic comparative investigations incorporating a limited amount of phenotype data can yield valuable insights into the adaptation of organismal systems to different environments.

ACKNOWLEDGMENTS

We express our sincere gratitude to T. Pietsch for his support and encouragement during all phases of this study. We also thank A. Bentley, K. Maslenikov, K. Hartel, and M. Vecchionne who provided gifts of tissue or opportunities to collect tissue biopsies. We are grateful to J. Orr, D. Stevenson, J. Felsenstein, and G. Lauder who made helpful comments on an earlier draft of the manuscript, along with L. Hauser who also provided laboratory space. We extend special gratitude to three anonymous referees whose critical comments were insightful and improved the manuscript greatly. E. Widder kindly provided the image in Figure 1B.

DATA ARCHIVING

Novel nucleotide sequences were accessioned in GenBank (accession no. KC163301–KC163334).

LITERATURE CITED

Betancur-R, R., R. E. Broughton, E. O. Wiley, K. Carpenter, J. A. López, C. Li, N. I. Holcroft, D. Arcila, M. Sanciangco, and J. C. Cureton II. 2013. The tree of life and a new classification of bony fishes. PLoS Curr. 5. doi: 10.1371/currents.tol.53ba26640df0ccaee75 bb165c8c26288.

Bowmaker, J. K., H. J. A. Dartnall, and P. J. Herring. 1988. Longwave-sensitive visual pigments in some deep-sea fishes: segregation of 'paired' rhodopsins and porphyropsins. J. Comp. Physiol. 163:685–698.

Carnevale, G. 2007. Fossil fishes from the Serravallian (Middle Miocene) of Torricella Peligna, Italy. Palaeontogr. Ital. 91:3–69.

Carnevale, G., and A. Rindone. 2011. The teleost fish *Paravinciguerria praecursor* Arambourg, 1954 in the Cenomanian of north-eastern Sicily. Boll. Soc. Paleontol. Ital. 50:1–10.

Chang, B. S. W., and D. L. Campbell. 2000. Bias in phylogenetic reconstruction of vertebrate rhodopsin sequences. Mol. Biol. Evol. 17:1220–1231.

Crane, J. M. 1966. Late Tertiatry radiation of viperfishes (Chauliodontidae) based on a comparison of recent and Miocene species. Los. Ang. Mus. Nat. Hist. Cont. Sci. 115:1–29.

Darriba, D., G. L. Taboada, R. Doallo, and D. Posada. 2011. ProtTest 3: fast selection of best-fit models of protein evolution. Bioinformatics 27:1164–1165.

Davis, M. P., and C. Fielitz. 2010. Estimating divergence times of lizardfishes and their allies (Euteleostei: Aulopiformes) and the timing of deep-sea adaptations. Mol. Phylogenet. Evol. 57:1194–1208.

Douglas, R. H., and J. C. Partridge. 1997. On the visual pigments of deep-sea fish. J. Fish Biol. 50:68–85.

Douglas, R. H., J. C. Partridge, and N. J. Marshall. 1998a. The eyes of deep-sea fish I: lens pigmentation, tapeta and visual pigments. Prog. Retin. Eye Res. 17:597–636.

Douglas, R. H., J. C. Partridge, K. Dulai, D. Hunt, C. W. Mullineaux, A. Y. Tauber, and P. H. Hynninen. 1998b. Dragon fish see using chlorophyll. Nature 393:423–424.

Drummond, A. J., B. Ashton, M. Cheung, J. Heled, M. Kearse, R. Moir, S. Stones-Havas, T. Thierer, and A. Wilson. 2009. Geneious v4.6. Biomatters, Auckland, New Zealand.

Drummond, A. J., and A. Rambaut. 2007. BEAST: Bayesian evolutionary analysis by sampling trees. BMC Evol. Biol. 7:214.

Drummond, A. J., S. Y. W. Ho, M. J. Phillips, and A. Rambaut. 2006. Relaxed phylogenetics and dating with confidence. PLoS Biol. 4:e88.

Edgar, R. C. 2004. MUSCLE: multiple sequence alignment with high accuracy and high throughput. Nucl. Acids Res. 32:1792–1797.

Eschmeyer, W. N. 2013. Catalog of fishes. California Academy of Sciences, San Francisco, CA. Available at http://www.calacademy.org/research/ichthyology/catalog/index.html.

Fernandez, H. R. 1979. Visual pigments of bioluminescent and nonbioluminescent deep-sea fishes. Vis. Res. 19:589–592.

Fink, W. L. 1985. Phylogenetic interrelationships of the stomiid fishes (Teleostei: Stomiiformes). Misc. Publ. Mus. Zool., Univ. Mich. 171:1–127.

Fink, W. L., and S. H. Weitzman. 1982. Relationships of the stomiiform fishes (Teleostei), with a description of *Diplophos*. Bull. Mus. Comp. Zool., Harvard Univ. 150:31–93.

Fitzgibbon, J., A. Hope, S. J. Slobodyanyuk, J. Bellingham, J. K. Bowmaker, and D. M. Hunt. 1995. The rhodopsin-encoding gene of bony fish lacks introns. Gene 164:273–277.

Gibbs, R. H. J., T. A. Clarke, and J. R. Gomon. 1983. Taxonomy and distribution of the stomioid fish genus *Eustomias* (Melanostomiidae), I: subgenus *Nominostomias*. Smithson. Contrib. Zool. 380:1–139.

Harms, M. J., and J. W. Thornton. 2010. Analyzing protein structure and function using ancestral gene reconstruction. Curr. Opin. Struct. Biol. 20:360–366.

Harold, A. S. 1998. Phylogenetic relationships of the Gonostomatidae (Teleostei: Stomiiformes). Bull. Mar. Sci. 62:715–741.

Harold, A. S., and S. H. Weitzman. 1996. Interrelationships of stomiiform fishes. Pp. 333–353 *in* M. L. J. Stiassny, L. R. Parenti, and G. D. Johnson, eds. Interrelationships of fishes. Academic Press, San Diego.

Hasegawa, E. I., K. Sawada, K. Abe, K. Watanabe, K. Uchikawa, Y. Okazaki, M. Toyama, and R. H. Douglas. 2008. The visual pigments of a deep-sea myctophid fish *Myctophum nitidulum* Garman; an HPLC and spectroscopic description of a non-paired rhodopsin–porphyropsin system. J. Fish Biol. 72:937–945.

Herring, P. J. 1983. The spectral characteristics of luminous marine organisms. Proc. Biol. Sci. 220:183–217.

———. 2007. Sex with the lights on? A review of bioluminescent sexual dimorphism in the sea. J. Mar. Biol. Assoc. 87:829–842.

Huddleston, R. W., and G. T. Takeuchi. 2013. Pp. 30–42. A new late Miocene species of sciaenid fish, based primarily on an in situ otolith from California. Bull. South. Calif. Acad. Sci. 105:30–42.

Hunt, D. M., K. S. Dulai, J. C. Partridge, P. Cottrill, and J. K. Bowmaker. 2001. The molecular basis for spectral tuning of rod visual pigments in deep-sea fish. J. Exp. Biol. 204:3333–3344.

Kenaley, C. P. 2008. Diel vertical migration of the loosejaw dragonfishes (Stomiiformes: Stomiidae: Malacosteinae): a new analysis for rare pelagic taxa. J. Fish Biol. 73:888–901.

———. 2010. Comparative innervation of cephalic photophores of the loosejaw dragonfishes (Teleostei: Stomiiformes: Stomiidae): evidence for parallel evolution of long-wave bioluminescence. J. Morphol. 271:418–437.

Knowles, L. L., and L. S. Kubatko. 2010. Estimating species trees: an introduction to concepts and models. Estimating species trees: practical and theoretical aspects. Wiley-Blackwell, Hoboken, NJ.

Le, S. Q., and O. Gascuel. 2008. An improved general amino acid replacement matrix. Mol. Biol. Evol. 25:1307–1320.

Li, C., G. Lu, and G. Orti. 2008. Optimal data partitioning and a test case for ray-finned fishes (Actinopterygii) based on ten nuclear loci. Syst. Biol. 57:519–539.

López, J. A., W.-J. Chen, G. Orti, and R. M. Wood. 2004. Esociform phylogeny. Copeia 2004:449–464.

Luterbacher, H. P., J. R. Ali, H. Brinkhuis, F. M. Gradstein, J. J. Hooker, S. Monechi, J. Powell, U. Röhl, A. Sanfilippo, and B. Schmitz. 2004. The Paleogene period. Pp. 384–408 *in* F. M. Gradstein, J. G. Ogg, and A. G. Smith, eds. A geological time scale 2004. Cambridge Univ. Press, Cambridge.

Marshall, C. R. 2008. A simple method for bracketing absolute divergence times on molecular phylogenies using multiple fossil calibration points. Am. Nat. 171:726–742.

Menon, S. T., M. Han, and T. P. Sakmar. 2001. Rhodopsin: structural basis of molecular physiology. Physiol. Rev. 81:1659–1688.

Morrow, J. E. J., and R. H. J. Gibbs. 1964. Family Melanostomiatidae. Pp. 351–522 *in* H. B. Bigelow, C. M. Breder, D. M. Cohen, G. W. Mead, D. Merriman, Y. H. Olsen, W. C. Schroeder, L. P. Schultz, and J. Tee-Van, eds. Fishes of the Western North Atlantic. Yale University, New Haven.

Near, T. J., R. I. Eytan, A. Dornburg, K. L. Kuhn, J. A. Moore, M. P. Davis, P. C. Wainwright, M. Friedman, and W. L. Smith. 2012. Resolution of ray-finned fish phylogeny and timing of diversification. Proc. Natl. Acad. Sci. USA 109:13698–13703.

Near, T. J., A. Dornburg, R. I. Eytan, B. P. Keck, W. L. Smith, K. L. Kuhn, J. A. Moore, S. A. Price, F. T. Burbrink, M. Friedman, and P. C. Wainwright. 2013. Phylogeny and tempo of diversification in the superradiation of spiny-rayed fishes. Proc. Natl. Acad. Sci. USA 110:12738–12743.

Nelson, J. S. 2006. Fishes of the world. 4th ed. John Wiley and Sons, New York.

Nylander, J. 2004. MrModeltest. Program distributed by the author, Evolutionary Biology Centre. Uppsala University, Uppsala, Sweden.

O'Day, W. T., and H. R. Fernandez. 1974. *Aristostomias scintillans* (Malacosteidae): a deep-sea fish with visual pigments apparently adapted to its own bioluminescence. Vis. Res. 14:545–550.

Paradis, E., J. Claude, and K. Strimmer. 2004. APE: analyses of phylogenetics and evolution in R language. Bioinformatics 20:289–290.

Partridge, J. C., S. N. Archer, and J. N. Lythgoe. 1988. Visual pigments in the individual rods of deep-sea fishes. J. Comp. Physiol. 162:543–550.

Partridge, J. C., S. N. Archer, and J. Vanoostrum. 1992. Single and multiple visual pigments in deep-sea fishes. J. Mar. Biol. Assoc. UK. 72:113–130.

Partridge, J. C., and R. H. Douglas. 1995. Far-red sensitivity of dragon fish. Nature 375:21–22.

Partridge, J. C., J. Shand, S. N. Archer, and J. N. Lythgoe. 1989. Interspecific variation in the visual pigments of deep-sea fishes. J. Comp. Physiol. A 164:513–529.

Piechnick, R., E. Ritter, P. W. Hildebrand, O. P. Ernst, P. Scheerer, K. P. Hofmann, and M. Heck. 2012. Effect of channel mutations on the uptake and release of the retinal ligand in opsin. Proc. Natl. Acad. Sci. USA 109:5247–5252.

R Core Team (2012). R: a language and environment for statistical computing. R Foundation for Statistical Computing, Vienna, Austria. ISBN 3–900051–07–0, Available at http://www.R-project.org/.

Rennison, D. J., G. L. Owens, and J. S. Taylor. 2011. Opsin gene duplication and divergence in ray-finned fish. Mol. Phylogenet. Evol. 62:986–1008.

Ronquist, F., and J. P. Huelsenbeck. 2003. MrBayes 3: Bayesian phylogenetic inference under mixed models. Bioinformatics 19:1572–1574.

Sanderson, M. J. 2002. Estimating absolute rates of molecular evolution and divergence times: a penalized likelihood approach. Mol. Biol. Evol. 19:101–109.

Schliep, K. P. 2011. phangorn: phylogenetic analysis in R. Bioinformatics 27:592–593.

Scopelliti, G., A. Bellanca, E. Erba, H. C. Jenkyns, R. Neri, P. Tamagnini, V. Luciani, and D. Masetti. 2008. Cenomanian–Turonian carbonate and organic-carbon isotope records, biostratigraphy and provenance of a key section in NE Sicily, Italy: palaeoceanographic and palaeogeographic implications. Palaeogeogr. Palaeoclimatol. Palaeoecol. 265: 59–77.

Sugawara, T. 2005. Parallelism of amino acid changes at the RH1 affecting spectral sensitivity among deep-water cichlids from Lakes Tanganyika and Malawi. Proc. Natl. Acad. Sci. USA 102:5448–5453.

Sugawara, T., Y. Terai, and N. Okada. 2002. Natural selection of the rhodopsin gene during the adaptive radiation of east african great lakes cichlid fishes. Mol. Biol. Evol. 19:1807–1811.

Sutton, T. T., and T. L. Hopkins. 1996a. Species composition, abundance, and vertical distribution of the stomiid (Pisces: Stomiiformes) fish assemblage of the Gulf of Mexico. Bull. Mar. Sci. 59:530–542.

———. 1996b. Trophic ecology of the stomiid (Pisces: Stomiidae) fish assemblage of the eastern Gulf of Mexico: strategies, selectivityand impact of a top mesopelagic predator group. Mar. Biol. 127:179–192.

Turner, J. R., E. M. White, M. A. Collins, J. C. Partridge, and R. H. Douglas. 2009. Vision in lanternfish (Myctophidae): adaptations for viewing bioluminescence in the deep-sea. Deep-Sea Res. Pt. I 56:1003–1017.

Warrant, E. J., and N. A. Locket. 2004. Vision in the deep sea. Biol. Rev. 79:671–712.

Weitzman, S. H. 1967. The origin of the stomiatoid fishes with comments on the classification of salmoniform fishes. Copeia 1967:507–540.

Xia, X., Z. Xie, M. Salemi, L. Chen, and Y. Wang. 2003. An index of substitution saturation and its application. Mol. Phylogenet. Evol. 26:1–7.

Yang, Z. 2007. PAML 4: phylogenetic analysis by maximum likelihood. Mol. Biol. Evol. 24:1586–1591.

Yang, Z., and M. dos Reis. 2011. Statistical properties of the branch-site test of positive selection. Mol. Biol. Evol. 28:1217–1228.

Yokoyama, S. 1995. Amino acid replacements and wavelength absorption of visual pigments in vertebrates. Mol. Biol. Evol. 12:53–61.

———. 2000a. Color vision of the coelacanth (*Latimeria chalumnae*) and adaptive evolution of rhodopsin (RH1) and rhodopsin-like (RH2) pigments. J. Hered. 91:215–220.

———. 2000b. Molecular evolution of vertebrate visual pigments. Prog. Retin. Eye Res. 19:385–419.

Yokoyama, S., and R. Yokoyama. 1996. Adaptive evolution of photoreceptors and visual pigments in vertebrates. Annu. Rev. Ecol. Syst. 27:543–567.

Yokoyama, S., N. Takenaka, and N. Blow. 2007. A novel spectral tuning in the short wavelength-sensitive (SWS1 and SWS2) pigments of bluefin killifish (*Lucania goodei*). Gene 396:196–202.

Yokoyama, S., T. Tada, H. Zhang, and L. Britt. 2008. Elucidation of phenotypic adaptations: molecular analyses of dim-light vision proteins in vertebrates. Proc. Natl. Acad. Sci. USA 105:13480–13485.

Associate Editor: T. Near

Supporting Information

Additional Supporting Information may be found in the online version of this article at the publisher's website:

Table S1. Sampled taxa of the family Stomiidae and tissue-sample voucher and GenBank accession numbers.
Table S2. Primers used in PCR amplification and sequencing.
Table S3. Nucleotide substitution models chosen under Akaike Information Criterion (AIC) as calculated in MrModelTest version 2.2 (Nylander 2004).
Figure S1. Phylogeny based on Bayesian analyses of ectodermal-neural cortex 1 (enc1).
Figure S2. Phylogeny based on Bayesian analyses of myosin, heavy chain 6, cardiac muscle, alpha (myh6).
Figure S3. Phylogeny based on Bayesian analyses of recombination activation gene 1 (rag1).
Figure S4. Phylogeny based on Bayesian analyses of rod opsin.
Figure S5. Phylogeny based on Bayesian analyses of enc1, myh6, rag1, and rod opsin.
Figure S6. Marginal ancestral state reconstructions of rod-opsin tuning sites plotted over a Bayesian-inferred phylogeny of stomiid dragonfishes and selected outgroups.
Appendix S1. Custom R script that generated ancestral state reconstructions depicted in Figure S6.
Appendix S2. Custom R script for "pheno.tip," code that generates estimations of rhodopsin phenotype based on share phylogenetically distinct sequence motifs.